Analytical Methods

Accepted Manuscript

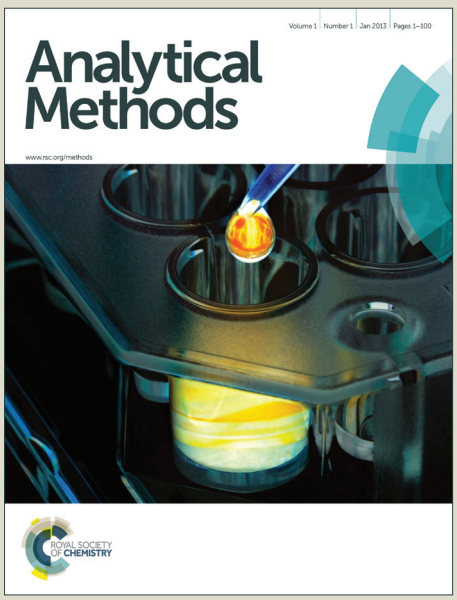

ROYAL SOCIETY OF CHEMISTRY

www.rsc.org/methods

Cite this: DOI: 10.1039/c0xx00000x

www.rsc.org/xxxxxx

PAPER

Sequential detection of Fe^{3+} and As^{3+} ions by naked eye through aggregation and dis-aggregation of biogenic gold nanoparticles

Somasundaram Kaviya and Edamana Prasad *

Received (in XXX, XXX) Xth XXXXXXXXX 20XX, Accepted Xth XXXXXXXXX 20XX
DOI: 10.1039/b000000x

We have synthesized and stabilized spherical, flower, urchin and polydispersed AuNPs using pomegranate (*Punica granatum*) peel extract. The AuNPs act as sequential sensors towards Fe^{3+} as well as As^{3+} ions. Upon addition of Fe^{3+} ions, the AuNPs aggregates due to the interaction between the capping agent and Fe^{3+} ions. The aggregation results in a color change visible to naked-eye, which is originated by the inter-plasmon coupling of AuNPs. Interestingly, the AuNP-Fe system dis-aggregates only in presence of As^{3+} ions, resulting further color change in the visible region. The aggregation and dis-aggregation phenomena were examined by UV-vis spectrophotometer, DLS, SEM, and TEM. The rates for aggregation and dis-aggregation of AuNP systems in presence of the metal ions were determined. The naked eye detection limit for Fe^{3+} and As^{3+} ions was 10^{-7} and 10^{-4} M, respectively. Finally, we have demonstrated the practical application of biosynthesized AuNPs by real sample analysis.

Introduction

Size and shape selective synthesis of gold nanoparticles (AuNPs) have gained significant attention because of its wide range of applications in the fields of sensors,[1] water purification,[2] surface enhanced Raman study (SERS),[3] catalysis,[4] antimicrobial research,[5] and drug delivery.[6] For example, spherical sized, relatively smaller NPs were effective for catalyzing the reduction of *p*-nitrophenol.[7] In an elegant study, Halas and co-workers have demonstrated the shape effects of gold nanosystems by comparing the release kinetics of DNA from gold nanorods and gold nanoshells. The results indicated that controlled release kinetics was obtained from gold nanorods.[8] Dong and their group reported the shape dependent SERS using gold nanowire network, nanoflower array, nanosheets and nanoflowers, where, nanoflower array exhibited relatively stronger SERS signals.[9] Studies revealed that smaller sized, spherical AuNPs show higher cellular uptake and penetration into the cancer cells compared to Au nanorods.[10,11]

Various physical,[12] chemical[3] and biological[4] methods have been utilized to synthesis NPs with different sizes and shapes. Among the biological methods, use of plant or plant fractions as a source for synthesizing NPs[4,13] were highly preferred, over other biological materials such as alga,[14] or fungus[15] because the later requires elaborate process of maintaining cell cultures. The present study described the use of pomegranate (*Punica granatum*) peel extract for the biosynthesis of AuNPs with different sizes and shapes. While pomegranate peel extract has been used to stabilise AuNPs,[16] the effect of pomegranate peel extract as a capping agent to generate AuNPs with varied size and shape has not been investigated. More importantly, we have utilized the Au NP systems stabilized by peel extract for naked eye detection of Fe^{3+} ions (10^{-7} M). Further, the sensor-analyte system (Au-Fe^{3+}) was utilized for a subsequent colorimetric selective detection of As^{3+} ions (10^{-4} M) in aqueous solution. While large number of metal NP based sensors are available towards toxic ions, generating a color change, observed by naked eye, for sequential detection of Fe^{3+} and As^{3+} ions at ambient conditions has not been demonstrated so far. We have utilized UV-visible spectrometer, dynamic light scattering technique (DLS), scanning electron microscope (SEM), and transmission electron microscope (TEM) for characterizing and analyzing the nanosystems. The kinetic studies provide invaluable information regarding the mechanistic aspect of the sensing process. The rate of aggregation and dis-aggregation process involved in the sensing mechanism has also been determined.

Experimental

Materials

All the chemicals were purchased from Sigma-Aldrich (USA) and used as received without further purification. Doubly distilled water was used for the experiments. Fresh and ripened pomegranate was purchased from the local market at Chennai (TN, India).

Preparation of the extract

Pomegranate peels were removed and washed with distilled water before and after peeling. About 2 g of peels were transferred into a clean beaker containing 100 mL of distilled water and boiled for 5 min. The extract was filtered using Whatman filter paper No 40 and stored in the refrigerator for further use.

Synthesis of gold nanoparticles with different shapes

Aqueous solution of $HAuCl_4$ (10 mL) was prepared in four different concentrations (concentration ranges between 10^{-2} M to 10^{-5} M). 200 µL of the extract was added to each solution of $HAuCl_4$ at room temperature. After the addition of the extract, the reaction mixture was mixed by shaken prior to the experiment.

Characterization

UV-visible spectroscopic studies were recorded on UV-3100 Hitachi spectrometer. The IR spectra have been taken using Perkin Elmer FT-IR spectrometer. Zeta potential and particle size measurements were carried out using zeta sizer (Malvern). The size and morphology of AuNPs were examined using scanning electron microscopy (SEM) (FEI Quanta FEG 200) and transmission electron microscopy (TEM) (Philips Tecnai 12). Energy dispersive X-ray spectroscopy (EDAX) and selective area electron diffraction (SAED) analysis were performed by TEM, equipped with an EDAX and SAED attachment. Bruker D8 advance powder X-day diffractometer with Cu Kα radiation was used for X-ray diffraction analysis. Inductively coupled plasma-optical emission spectroscopy (ICP-OES) measurements were carried out using Perkin Elmer Optima 5300 DV. The photographs were taken with Canon A3200 IS digital camera.

Colorimetric assay

Colorimetric detection experiments in presence of various metal ions (Na^+, K^+, Li^+, Ca^{2+}, Cu^{2+}, Mg^{2+}, Mn^{2+}, Co^{2+}, Zn^{2+}, Ni^{2+}, Pb^{2+}, Cd^{2+}, Hg^{2+}, UO_2^{2+}, Ba^{2+}, Fe^{2+}, Bi^{3+}, Fe^{3+}, As^{3+}, Al^{3+}, Cr^{3+}, Ce^{4+}, V^{4+}, As^{5+}) were performed in aqueous solution by biosynthesized AuNPs (1 to 4) at room temperature. The concentration of Fe^{3+} and As^{3+} ions were varied from 10^{-1} M to 10^{-7} M and 10^{-1} M to 10^{-4} M, respectively. 100 µL of metal ion was added to 200 µL of AuNPs, along with the addition of ~ 1 mL of water. The sensing and selectivity of the metal ions were monitored using UV-vis absorption spectroscopy by changes in the surface plasmon resonance (SPR) peak of AuNPs.

Kinetic studies

The kinetic experiments were carried out by monitoring the changes in absorption band of AuNP in presence of the metal ions (Fe^{3+} and As^{3+}), under pseudo first order conditions. The rate constants were determined using graphical methods where observed rate constants were plotted against concentrations of the analyte metal ions.

Results and Discussion

Our aim is to synthesis gold nanoparticle with different sizes and shapes in order to find the impact of size/shape variations on toxic metal ion sensing. Detection of toxic metal ions in water is important because imbalance in the concentration of such species can lead to a number of diseases.[17-20]

Pomegranate peels have been used in folk medicine for the remedy of dysentery, diarrhea and stomatitis.[21,22] The peels are rich in tannins and polyphenols[23-25] and they have also been used in anti-cancer, anti-inflammatory, antihelminthic treatments.[26,27] We hypothesized that the presence of polyphenols in the peel extract can potentially reduce the gold ions and the available amino acids/poly peptides can stabilize the nanosystems by steric effect.

We also hypothesized that the presence of various functional groups in pomegranate peel extract can also be used to sense toxic metal ions.

Factors affecting the size and shape of AuNPs

Initially, we fixed the concentration of $HAuCl_4$ (10^{-3} M) (10 mL) and varied the amount of peel extract from 100 µL to 1 mL. We observed that the AuNP solution formed was red in color and the color did not change as a function of the peel extract concentration. However, UV-vis spectra of the solutions exhibit slight spectral broadening as the concentration of the peel extract increases (Fig. S1). Since SPR band maxima remains the same in these experiments, formation of AuNPs with different shapes is less likely. The TEM analysis also corroborates this hypothesis (vide infra). The variable concentration study suggest that 200 µL of the extract provides the optimum condition for getting smaller sized spherical NPs from 10^{-3} M $HAuCl_4$. The spectral broadening also suggests that aggregation propensity of the NP increases as the concentration of the peel extract increases >200µl. Conversely, increasing the concentration of $HAuCl_4$ from 10^{-5} to 10^{-2} M, keeping the peel extract concentration identical (200 µL), results in a clear shift in the SPR absorption maxima (Fig. 1). This indicates drastic changes in the size and/or shape of the NPs as a function of the metal precursor. The TEM analysis supports this hypothesis and the images clearly exhibit polydispersed, spherical, flower and urchin shaped NPs for different concentrations of the NP precursor (Fig. 2 and Fig. S2). The experiments were reproduced four times and identical TEM images were obtained. From the above results, it is concluded that the size and shape of the NPs can be controlled by keeping the concentration of the peel extract identical (200 µL in the present case) and varying the concentration of the metal ion precursor.

Upon the addition of the extract (200 µL) to different concentrations of $HAuCl_4$ solutions (10^{-2} to 10^{-5} M), the color of the solutions changed from pale yellow to violet, red, blue and ash within one minute. The solutions are respectively named as AuNP1, AuNP2, AuNP3 and AuNP4. The UV-vis absorption spectra of AuP1 to AuP4 solutions are shown in Fig. 1, along with the corresponding photographs (Fig. 1 inset).

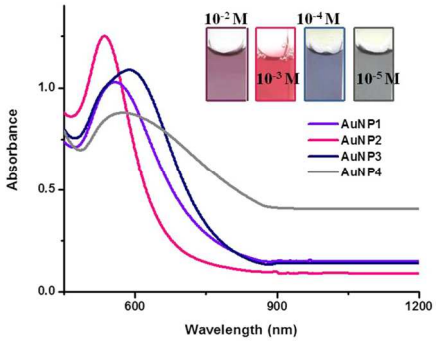

Fig. 1 UV-vis spectra of AuNPs synthesized at different concentrations of $HAuCl_4$ (10^{-2} to 10^{-5} M). (The as-synthesised AuNPs are represented as: AuNP1 (10^{-2} M), AuNP2 (10^{-3} M), AuNP3 (10^{-4} M) and AuNP4 (10^{-5} M).

AuNP2 exhibits a sharp absorption, compared to other solutions indicating that spherical and uniform sized AuNPs were generated. The red shift in the SPR peak for AuNP3 and AuNP4

indicates that there is a relative increment in the particle size.[28] A careful analysis of the TEM images indicates that AuNP1 contains spherical, triangular and hexagonal shaped particles (Fig. 2a). Conversely, all the nanoparticles in AuNP2 are spherical, well dispersed and uniform in size (~ 20 nm) and shape (Fig. 2b). The shapes of AuNP3 and AuNP4 are flower and urchin, respectively. While these NPs are monodispersed, they have increased size (~50 and 100 nm, respectively), which is consistent with the UV-vis study (Fig. 2c & d).

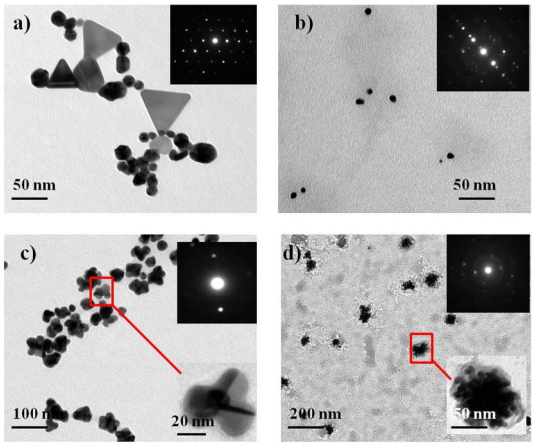

Fig. 2 TEM images of a) AuNP1, b) AuNP2, c) AuNP3 and d) AuNP4. Insets are the corresponding SAED images.

SAED patterns of pomegranate peel extract stabilized AuNPs are given in the inset of Fig. 2. The image reflects the (111), (200), (220) and (311) diffraction pattern which indicates the *fcc* structure of AuNPs. The presence of elemental gold is confirmed by EDX analysis. It shows a strong peak of Au at 2.2 KeV, which is characteristic of AuNPs (Fig. S3).[29] XRD patterns of AuNPs (1-4) were recorded by drop casting of the solution on glass slides. The Bragg's reflection (111), (200), (220) and (311) were clearly observed (Fig. S4) which also indicates the *fcc* structure of the AuNPs,[30] consistent with SAED pattern.

Next, we have carried out dynamic light scattering and zeta potential measurements for the synthesized monodispersed nanoparticles. The results are summarized in Table S1. It is shown that, the zeta potential of the nanoparticles follows the order AuNP2 < AuNP3 < AuNP4 and the nanoparticles are negatively charged on the surface (AuNP1 was not analysed for zeta potential measurements due to the presence of polydispersed particles). The hydrodynamic radius also follows the order AuNP2 < AuNP3 < AuNP4.

Mechanism for the formation of NPs

Pomegranate peels are richer in phytochemicals. It is a richer source of tannins and phenolic compounds such as punicalagin and punicalin.[17-19] N-methyl granatonine is a coloring agent which is present in an alkaloid form in the aqueous extract of peels.[31] The functional groups present in the extract are confirmed by taking FT-IR spectrum of the peel extract where spectral bands ranging from 763 to 3342 cm^{-1} were observed (Fig. S5). The band at 3342 cm^{-1} is attributed to stretching vibration of O-H in phenolic groups of polyphenols. The peaks at 2926, 2315 and 2138 cm^{-1} are due to stretching vibrations of C-H and O-C-O groups. C=C stretching vibration is observed at 1644 cm^{-1} and the peaks at 1450, 1211, 1047 and 763 cm^{-1} are corresponding to stretching vibrations from C=C, C-O, C-OH, C-H groups, respectively. Fig. S6 shows the UV-vis absorption spectra of the aqueous peel extract. The peeks at 228, 256 and 374 nm exactly match with the spectra of phenolic compound punicalagin.[32] Hence, it can be concluded that these functional groups (-C=C-, CH_3, C=O, OH) present in the extract are responsible for the reduction and stabilization of the formed nanoparticles.[33]

The variation in size and shape of AuNPs can be explained based on the ratio between Au^{3+} ions and capping agent. When the ratio is relatively high, aggregation propensity will be high, leading to the formation of NP with various size and shapes. For example, AuNP1 system provides NP with various sizes and shapes due to the relatively high concentration of the Au^{3+} ions compared to the capping agent (i.e, high ratio between Au^{3+} and capping agent). On the other hand, the uniform size and shape in AuNP2 indicates that the amount of the capping agent and Au^{3+} ions is optimised so that aggregation propensity is controlled. When the ratio between Au^{3+} ions and capping agent is low, as in the case of AuNP3 and AuNP4, concentration of the capping agent is increased further, and the aggregation propensity of the systems also increases. This leads to flower and urchin shaped NPs. The fact that the size and shape of the NPs remain the same for AuNP3 and AuNP4 suggests that aggregation was controlled in nature.

Colorimetric naked eye detection of Fe^{3+} by AuNPs (1-4)

We have used the aqueous pomegranate peel extract stabilized AuNPs (1-4) for the colorimetric detection of metal ions in aqueous solution. AuNPs show size and shape dependent SPR, which are highly sensitive to selected analytes.[33,34] Depending on extent of aggregation, the shift of SPR may vary from visible to near-IR region.[35,36] In the present study, the selectivity of AuNP was investigated with twenty four different metal ions (Fig. 3, S7 & 8). We observed that, the NPs have exhibited a color change only in presence of Fe^{3+} ions, which can be observed by naked eye. Interestingly, the color change due to the presence of Fe^{3+} ions was unique in the four different AuNP systems. While AuNP1 shows a color variation from violet to brown, AuNP2 exhibits a color change from red to brown, in presence of Fe^{3+} ions. AuNP3 and AuNP4 show color change from blue to ash and ash to black, respectively. The above color changes are due to the formation of different sized AuNP aggregates in presence of Fe^{3+} ions, which are confirmed by UV-vis spectroscopy. The intensity of SPR band for AuNP1 and AuNP2 is decreased in presence of Fe^{3+} ions, with the concomitant increase of two SPR band at ~ 700 nm and ~ 1060 nm (Fig. S9a & b). The intensity of the SPR peaks of AuNP3 and AuNP4 were also decreased as Fe^{3+} ions concentration is increased, with the formation of an additional SPR band in the NIR region (Fig. S9c & d). Since the color contrast in AuNP2 and AuNP3 is relatively high in presence of Fe^{3+} ions, the naked eye detection of Fe^{3+} ions was feasible for solution as dilute as 10^{-7}M.

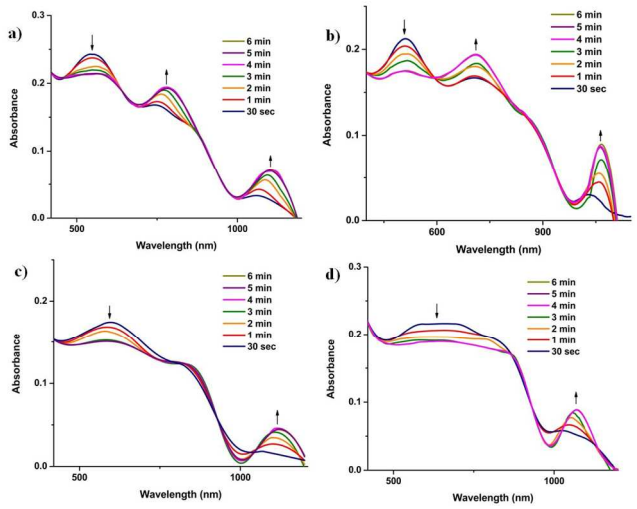

Fig. 3 The time dependent aggregation of a) AuNP1, b) AuNP2, c) AuNP3 and d) AuNP4 monitored by UV-vis absorption in presence of 10^{-6} M [Fe^{3+}].

Morphological changes of AuNPs induced by Fe^{3+} ions were examined through scanning electron microscopy (SEM) and transmission electron microscopy (TEM). Addition of Fe^{3+} ions (10^{-6} M) to AuNP solution triggers NP aggregation as evident from the TEM image (Fig. 4). Careful examination of TEM images indicates the formation alloy NPs and core@shell NPs[37-39] in AuNP2 (Fig 4b & S10). We also observed that the formation of core@shell NPs are less compared to that of alloy NPs in the case of AuNP2. In the presence of Fe^{3+} ions, AuNP3 and AuNP4

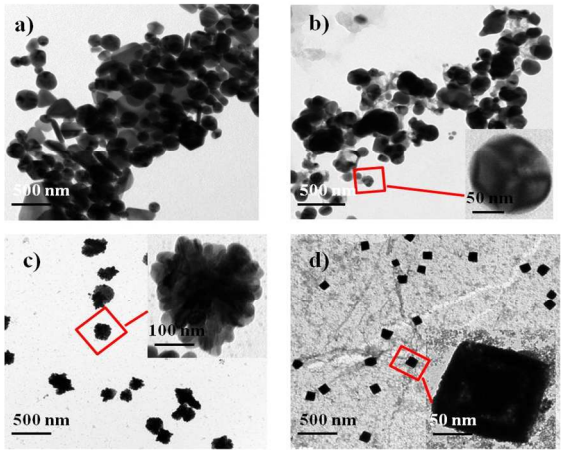

Fig. 4 TEM images of a) AuNP1, b) AuNP2, c) AuNP3 and d) AuNP4 in presence of Fe^{3+} ions (10^{-6} M). The images are taken after 2 min of addition.

systems form urchin and cubic shape aggregates in solution (Fig. 4c & d). The formation of alloy or core-shell NPs depends on the distribution of Fe^{3+} ions on the surface of AuNPs.[40] The fact that SPR band in AuNP systems shift from visible to IR region upon addition of Fe^{3+} ions suggests that the metal ion binds with the biomolecules on the surface of the NPs and bring them together resulting in inter-plasmonic coupling interactions.[32-39, 41-44] The aggregation propensity of the NPs depends on the concentration of metal ion, the binding nature of the functional groups on the NP surface, size and shape of the NPs.

The centrifuged sample was taken for XRD analysis and diffraction peaks at 33.13, 35.64, 40.89, 54.10, 57.59 and 62. 47 are indexed as (104), (110), (113), (116), (018) and (214) (Fig. S11).These reflections correspond to rhombohedral structure of α-Fe_2O_3[43]. This indicates that, Fe^0 is oxidized to α-Fe_2O_3 NPs in all the four different AuNPs.[40] The presence of iron in the aggregates, was also confirmed by EDAX analysis (Fig. S12). These results are consistent with the XRD analysis. We investigated the effect of other metal ion on AuNP and Fe^{3+} system. The result suggests that, there is no change in the SPR absorption of AuNPs in presence of other metal ions (except As^{3+} ion) (Fig. S13).

Rate of aggregation of AuNPs (1-4) by Fe^{3+}

We have monitored the time dependent changes in the absorption of AuNPs in presence of Fe^{3+} ions. UV-vis spectra show that, upon addition of Fe^{3+} ions, the peak intensity of AuNPs at ~550 nm is decreased and the intensity of additional peaks in the visible and NIR regions are enhanced, presumably due to aggregation of NPs (Fig. 3). It is also noticed that the intensity of the additional peaks is enhanced and reached a plateau after four minutes. Similarly, time dependent DLS experiments suggest that aggregation reaches a saturated level after four minutes (Fig. S14 &15). The changes in the size and shape of the AuNP-Fe aggregates were also monitored by time dependent SEM and TEM. The morphology of AuNP1, AuNP2, AuNP3, and AuNP4 has been changed from their respective initial structures to dendritic (Fig. S16 b), flower (Fig. S16 d), sheet (Fig. S17 b) and flower bouquet (Fig. S17 d).

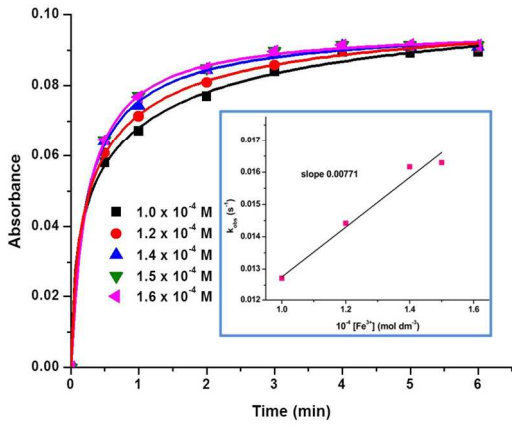

Fig. 5 *Logistic* growth fitting for time dependent aggregation of AuNP4 with the addition of different concentration of Fe^{3+} ions. Inset shows the linear fitting of observed rate constant vs different concentration of Fe^{3+} ions.

In order to find out the rate of aggregation of AuNPs in presence of Fe^{3+} ions, rate studies have been carried out under *pseudo*-first-order conditions, by keeping [Fe^{3+}] in excess (>10 times). The time dependent changes of the SPR of the NPs were

monitored using UV-vis spectrometer. All the AuNP systems have shown *logistic* growth of aggregation (Fig. 5 & S18). We found the observed rate constant from the *logistic* growth curve in absorbance vs time plot. Further, we found the bimolecular rate constant by the linear fitting of observed rate constants vs concentration of Fe^{3+} ions, which is given in Fig. S19. The bimolecular rate constant values for all the four AuNP- Fe systems are given in Table S2. The concentration of Fe^{3+} ion was changed from 1.0 x10^{-4} M to 1.6 x 10^{-4} M (Fig. 5 & S18).

Colorimetric naked eye sensing of As^{3+} by AuNP-Fe system

It is clear from the interference study that presence of As^{3+} ions affects the NIR absorption peak of AuNP-Fe system. In literature, reports are available for the sensing/adsorption of As^{3+} ions by iron, iron oxide NPs,[45-47] and Au/Au-Fe NPs modified electrodes.[48,49] However, relatively very few reports are available regarding As^{3+} sensing based on AuNPs[50] and Au nanoclusters.[51] Among the various metal ions examined, the addition of only As^{3+} (10^{-4} M) in AuNP-Fe system results in a drastic color change. The color change due to the presence of As^{3+} was detectable by naked-eye, as in the case of Fe^{3+} detection by the Au NP. We have monitored the absorption spectrum of AuNP-Fe system with twenty three different metal ions in aqueous solution (Fig. S12).

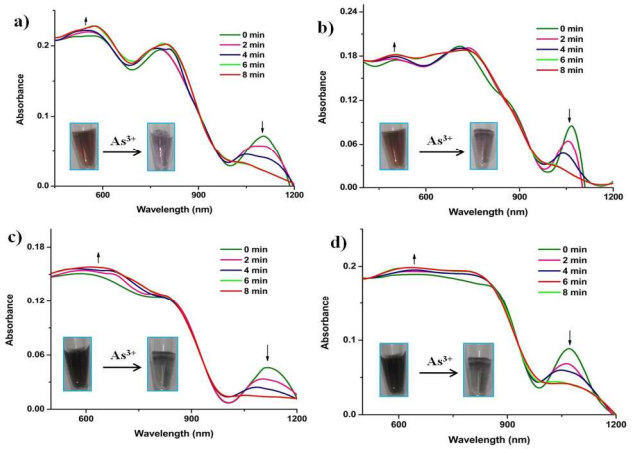

Fig. 6 UV-vis absorption spectra showing the time dependent disaggregation of a) AuNP1-Fe, b) AuNP2-Fe, c) AuNP3-Fe, d) AuNP4-Fe system in presence of 10^{-3} M of As^{3+} ions.

The UV-vis absorption spectra show that, upon addition of As^{3+} to AuNP-Fe system, the intensity of the SPR peak at near-IR region is decreased (Fig. 6 & S20) and the intensity of the SPR in the visible region is increased. This suggests that the AuNP-Fe dis-aggregates in presence of As^{3+} ions. The graph between the absorption vs time indicates that the dis-aggregation process followed an exponential decay (Fig. 7, S20). The rate of dis-aggregation of AuNPs-Fe system was determined by monitoring the SPR in presence of different concentration of As^{3+} in AuNP-Fe systems (Fig. 6 & S20). We found the dis-aggregation rate constant values for the systems by the linear fitting of observed rate constant vs different concentration of As^{3+} ions (inset, Fig. 7 and S21, Table S3). The disaggregation of AuNP-Fe with the addition of As^{3+} was also monitored by SEM and the images clearly show the fragmentation after addition of As^{3+} (Fig. S22-26). The disaggregation of AuNP-Fe system was further confirmed by time dependent DLS measurements. The result shows that, the size of the aggregates is decreased in presence of As^{3+} ions. The time taken for the size re-organization was close to that is observed by UV-vis spectrophotometer (Fig. S27 & 28).

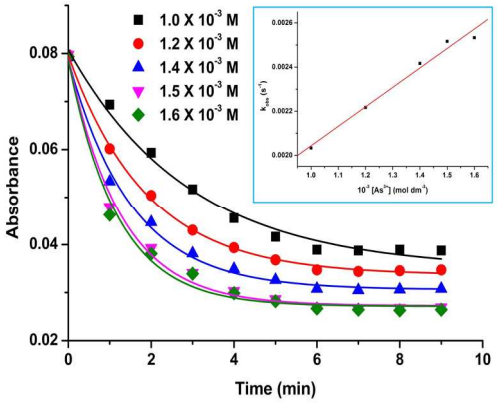

Fig. 7 Exponential decay fitting for the time dependent dis-aggregation of AuNP4 in presence of different concentration of As^{3+} ions. Inset shows the linear fitting of observed rate constant vs different concentration of As^{3+} ions.

It has been reported in the literature that strong interaction is likely to occur between As^{3+} and α-Fe_2O_3.[52] It is feasible that α-Fe_2O_3 could leach out due to the interaction, which is confirmed by XRD analysis of the aggregates (Fig. S29).[53]The disaggregation results again a color change/color disappearance. The detection limit for As^{3+} by naked–eye has been calculated as 10^{-4}M. Interference study was also carried out with other metal ions and the results suggest that, the AuNP-Fe system is selectively sensing As^{3+} ions (Fig. S30). The schematic representation of aggregation followed by disaggregation process is shown below (Scheme 1).

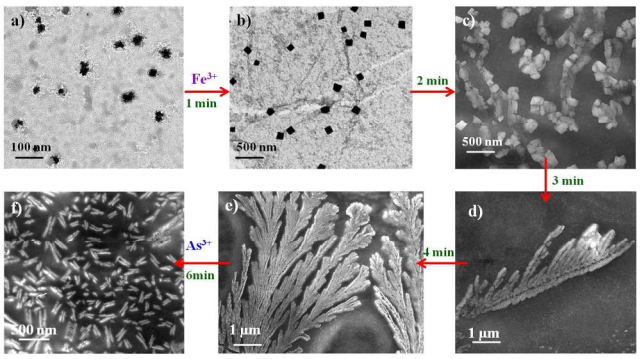

Fig. 8 TEM (a and b) and SEM (c-f) images are showing the aggregation and disaggregation of AuNP4 in presence of Fe^{3+} (10^{-6} M) and As^{3+} (10^{-3} M) ions.

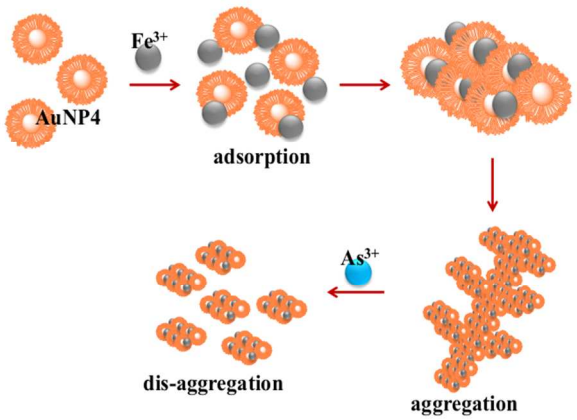

Scheme 1: Proposed mechanism for the aggregation and disaggregation of AuNP4 with the addition of Fe^{3+} and As^{3+} ions.

Application of AuNPs in real sample analysis

In order to test the sensing ability of the as-synthesized AuNP based system, tap water was collected and analysed using the NPs. Initially, the water sample was filtered through Whatman filter paper No 40 and then utilized for testing. About, 200 µL of tap water was added to 100 µL of different AuNPs (AuNP1-4). The color of the solution was changed upon keeping the solution for ten minutes and the UV-vis spectra indicate similar changes to that obtained in presence of Fe^{3+} ions (Fig. S31). The presence of Fe^{3+} ions in tap water was further confirmed by ICP-OES experiment and the amount was quantified as 0.012 mg/L. The results suggest that the as-synthesized AuNP system provides a cost effective way of detecting the presence of iron and arsenic by 'necked eye detection' for real-time water analysis.

Conclusion

In this work, we have synthesised and stabilized four different types of AuNPs using pomegranate peel extract. As-synthesized AuNP systems have been utilized to detect Fe^{3+} ions at 10^{-7} M of the analyte, leading to a definite color change in the visible region. The adsorbed Fe^{3+} ions form alloy as well as core-shell nanosystems with AuNPs. Furthermore, the AuNP-Fe systems were used to sense As^{3+} ions in aqueous solution via a reversible aggregation pathway. The sensing of As^{3+} ions can be monitored by naked eye and the detection limits was 10^{-4} M. The methods of NP synthesis and sequential metal ion sensing are simple, cost effective, time saving and eco-friendly. Finally, we demonstrated the practical application of these bio-NPs by analysis of tap water. The results taken together indicate that the presence of pomegranate peal extract is essential for the sequential detection of metal ions, due to its rich content of several functional groups.

Acknowledgment

S. Kaviya thanks for the INSPIRE fellowship from DST, Govt. of India. We thank the financial support from DST Nano Mission {Ref. No. SR/NM/MS-115/2010 (G)}.

Notes and references

Department of Chemistry, Indian Institute of Technology Madras, Chennai-600 036, TN, India. Fax: (+) 91-44-2257-4202; Tel: +91 44 2257 4232; E-mail: pre@iitm.ac.in (Edamana Prasad)

† Electronic Supplementary Information (ESI) available: See DOI: 10.1039/b000000x/

1. Y. H. Chien, C. C. Huang, S. W. Wang and C. S. Yeh, *Green Chem.*, 2011, **13**, 1162-1166.
2. S. K. Das, A. R. Das and A. K. Guha, *Langmuir*, 2009, **25**, 8192-8199.
3. C. M. MacLaughlin, N. Mullaithilaga, G. Yang, S. Y. Ip, C. Wang and G. C. Walker, *Langmuir*, 2013, **29**, 1908-1919.
4. V. Reddy, R. S. Torati, S. Oh and C. Kim, *Ind. Eng. Chem. Res*., 2013, **52**, 556-564.
5. D. Mubarakali, N. Thajuddin, K. Jeganathan, and M. Gunasekaran, *Colloids Surf. B*, 2011, **85,** 360-365.
6. C. K. Kim, P. Ghosh and V. M. Rotello, *Nanoscale*, 2009, **1**, 61-67.
7. S. K. Das, C. Dickinson, F. Lafir, D. F. Brougham and E. Marsili, *Green Chem.*, 2012, **14**, 1322-1334.
8. R. Huschka, J. Zuloage, M. W. Knight, L.V. Brown, P. Nordlander and N. J. Halas, *J. Am. Chem. Soc*., 2011, **133**, 12247-12255.
9. T. Wang, X. Hu and S. Dong, *J. Phys. Chem. B*, 2006, **110**, 16930-16936.
10. K. Huang, H. Ma, J. Liu, S. Huo, A. Kumar, T. Wei, X. Zhang, S. Jin, Y. Gan, P. C. Wang, S. He, X. Zhang and X. J. Liang, *ACS Nano*, 2012, **6**, 4483-4493.
11. C. Xu, D. Yang, L. Mei, B. Lu, L. Chen, Q. Li, H. Zhu and T. Wang, *ACS Appl. Mater. Interfaces*, 2013, **5**, 2715-2724.
12. D. Jang and D. Kim, *Appl. Phys. A*, 2004, **79,** 1985-1988.
13. S. Kaviya, J. Santhanalakshmi, B. Viswanathan, J. Muthumary and K. Srinivasan, *Spectrochim. Acta A*, 2011, **79**, 594-598.
14. K. Kalishwaralal, V. Deepak, S. R. K. Pandian, M. Kottaisamy, S. Barathmanikanth, B. Kartikeyan and S. Gurunathan, *Colloids Surf. B: Biointerfaces*, 2010, **77**, 257-262.
15. P. Mukherjee, A. Ahmad, D. Mandal, S. Senapati, S. R. Sainkar, M. I. Khan, R. Parishcha, P. V. Ajaykumar, M. Alam, R. Kumar, M. Sastry, *Nano Lett*., 2001, **1**, 515-519.
16. M. Ganeshkumar, M. Sathishkumar, T. Ponrasu, M. G. Dinesh and L. Suguna, *Colloids Surf. B: Biointerfaces*, 2013, **106**, 208-216.
17. J. R. Burdo and J. R. Connor, *BioMetals*, 2003, **16**, 63-75.
18. B. K. Mandal and K. T. Suzuki, *Talanta*, 2002, **58**, 201-235.
19. J. C. Saha, A. K. Dikshit, M. Bandyopadhyay and K. C. Saha, *Crit. Rev. Environ. Sci. Technol*., 1999, **29**, 281-313.
20. H. S. Yu, W. T. Liao and C. Y. Chai, *J. Biomed. Sci.*, 2006, **13**, 657-666.
21. K. Boukef, H. R. Souissi and G. Balansard, *Plant Medicine Phytothereapy*, 1982, **16**, 260-279.
22. A. Caceres, L. M. Giron, S. R. Alvarado and M. F. Torres, *Journal of Ethanopharmacolgy*, 1987, **20**, 223-237.
23. H. Saad, F. C. Bouhtoury, A. Pizzi, K. Rode, B. Charrier and N. Ayed, *Ind. Crop. Prod.,* 2012, **40**, 239-246.
24. M. Cam and Y. Hisil, *Food Chem*., 2010, **123**, 878-885.
25. T. Ismail, P. Sestili and S. Akhter, *J. Ethnopharmacol*., 2012, **143**, 397-405.
26. E. A. Hayouni, K. Miled, S. Boubaker, Z. Bellasfar, M. Abedrabbad, H. Iwaskie, H. Okue, T. Matsuie, F. Limama and M. Hamdi, *Phytomedicine*, 2011, **18**, 976-984.

27. G. Mousavinejad, Z. E. Djomeh, K. Rezaei and M. H. H. Khodaparast, *Food Chem.,* 2009, **115,** 1274-1278.
28. T. Sen and A. Patra, *J. Phys. Chem. C*, 2009, **113**, 13125-13132.
29. S. Das, A. R. Das and A. K. Guha, *Small*, 2010, **6**, 1012-1021.
30. N. Ozkal and S. Dinc, *Ankara Univ Eczacilik Fak Derg*, 1994, **22**, 21-29.
31. J. Moilanen, J. Sinkkonen and J. P. Salminen, *Chemoecology*, 2013, **23**, 165-179.
32. S. Kaviya and E. Prasad, *ACS Sustainable Chem. Eng.*, 2014, **2**, 699-705.
33. J. Schmitt, P. Machtle, D. Eck, H. Mohwald and C. A. Helm, *Langmuir*, 1999, **15**, 3256-3266.
34. P. Mulvaney, *Langmuir* 1996, **12**, 788-800.
35. S. P. Wu, Y.P. Chen and Y. M. Sung, *Analyst*, 2011, **136**, 1887-1891.
36. T. J. Norman, C. D. Grant, D. Magana and J. Z. Zhang, *J. Phys. Chem. B*, 2002, **106**, 7005-7012.
37. D. L. Lu, K. Domen and K. I. Tanaka, *Langmuir*, 2002, **18**, 3226-3232.
38. N. Dahal and V. Chikan, *Chem. Mater*, 2008, **20**, 6389-6395.
39. K. C. F. Leung, S. Xuan, X. Zhu, D. Wang, C. P. Chak, S. F. Lee, W. K. W. Ho and B. C. T. Chung, *Chem. Soc. Rev*., 2012, **41**, 1911-1928.
40. M. B. Cortie and A. M. M. Donagh, *Chem. Rev.*, 2011, **111**, 3713-3735.
41. H. Yu, M. Chen, P. M. Rice, S. X. Wang, R. L. White and S. Sun, *Nano Lett.*, 2005, **5**, 379-382.
42. A. Gole, J. W. Stone, W. R. Gemmill, H. C. Loye and C. J. Murphy, *Langmuir*, 2008, **24**, 6232-6237.
43. L. Zhou, H. Xu, H. Zhang, J. Yang, S. B. Hartono, K. Qian, J. Zou and C. Yu, *Chem. Commun*., 2013, **49**, 8695-8697.
44. H. Jans and Q. Huo, *Chem. Soc. Rev.*, 2012, **41**, 2849-2866.
45. N. Horzum, M. M. Demir, M. Nairat and T. Shahwan, *RSC Adv*., 2013, **3**, 7828-7837.
46. A. Gupta, M. Yunus and N. Sankararamakrishnan, *Ind. Eng. Chem. Res.*, 2013, **52**, 2066-2072.
47. C. Gao, X. Y. Yu, S. Q. Xiong, J. H. Liu and X. J. Huang, *Anal. Chem.*, 2013, **85**, 2673-2680.
48. X. Dai, O. Nekrassova, M. E. Hyde and R. G. Compton, *Anal. Chem.*, 2004, **76**, 5924-5929.
49. H. Cui, W. Yang, X. Li, H. Zhao and Z. Yuan, *Anal. Methods*, 2012, **4**, 4176-4181.
50. N. Xia, Y. Shi, R. Zhang, F. Zhao, F. Liu and L. Liu, *Anal. Methods*, 2012, **4**, 3937-3941.
51. S. Roy, G. Palui and A. Banerjee, *Nanoscale*, 2012, **4**, 2734-2740.
52. R. Prucek, J. Tucek, J. Kolarik, J. Filip, Z. Marusak, V. K. Sharma and R. Zboril, *Environ. Sci. Technol.*, 2013, **47**, 3283-3292.
53. S. K. Tripathy, J. Y. Woo and C. S. Han, *Sens. Actuators B. Chem.*, 2013, **181**, 114-118.